UK Atomic Energy Authority

UKAEA-STEP-PR(23)15

M. Anderton, C. Baus, T. P. Davis, R. Pearson, K. Mukai, J. Pollard, K. Taylor, S. Kirk, J. Hagues

Novel high temperature tritium breeder designs for confined spaces in spherical tokamaks fusion reactors

Novel high temperature tritium breeder designs for confined spaces in spherical tokamaks fusion reactors

M. Anderton, C. Baus, T. P. Davis, R. Pearson, K. Mukai, J. Pollard, K. Taylor, S. Kirk, J. Hagues

This is a preprint of a paper submitted for publication in Nuclear Fusion

Novel high temperature tritium breeder designs for confined spaces in spherical tokamaks fusion reactors⋆,⋆⋆

M. Anderton[a,*], C. Baus[b,c], T. P. Davis[a], R. Pearson[b,c], K. Mukai[b,c], J. Pollard[a], K. Taylor[d], S. Kirk[d] and J. Hagues[d]

[a]Oxford Sigma Ltd., Harwell Innovation Centre 173 Curie Avenue, Oxfordshire, OX11 0QG, United Kingdom,
[b]Kyoto University, Gokasho, Uji, 611-0011, Kyoto Japan
[c]Kyoto Fusioneering, Otemachi Bldg. 6th Floor Inspired.Lab, 1-6-1 Otemachi, Chiyoda-ku, 100-0004, Tokyo Japan
[d]United Kingdom Atomic Energy Authority (UKAEA), United Kingdom

ABSTRACT

Tritium self-sufficiency is one of the fundamental challenges for deuterium-tritium nuclear fusion reactors. The combination of key high temperature radiation shielding materials that possess dense, high neutron absorption cross-section, and moderation properties, and tritium breeding materials could involve interesting design spaces for the central column challenge in spherical tokamaks. Potential tungsten alloys can be used for two functions: radiation shielding and structural material, providing a new design space window for spherical tokamak central column breeding space. In this paper we present two novel high temperature concepts for the inboard side of the breeder blanket in a confined space. A tungsten-rhenium-hafnium-carbide lithium-based design was found to offer the best TBR given a parameter optimisation based on shielding and thermal requirements. A silicon-carbide lead-lithium breeder design was also investigated. The highest TBR was found to be 0.135 in a 3D neutronics calculation with a W-24.5Re-2HfC (structural and shielding, wt%), Li (90% Li-6 enriched breeder), and W_2B_5 (shielding) option.

1. Introduction

Fusion energy is a candidate for zero-carbon energy source for the future. Two hydrogen isotopes are used as fuels in fusion reactors, deuterium and tritium. Deuterium can be found in relative abundance in sea water. As a result of its extreme scarcity, nuclear fusion reactors require radioactive tritium to be bred online during operation in order to supply the fuel for the reactor's continued operation, via so-called tritium breeder blankets. These blankets contain lithium-6 (and lithium-7) which, upon interaction with a fusion neutron, will produce tritium, the hydrogen isotope used as fuel for a fusion reactor, thereby reproducing the fuel required for the fusion reactor in-situ. However, as a component that will surround the fusion reactor core, the breeder blanket will experience, inter alia, extreme radiation damage, high operational temperatures, large magnetic fields, and corrosion damage from coolants.

For commercial deployment, is vital that a fusion reactor produces sufficient tritium to sustain operation, defined as a reactor Tritium Breeding Ratio (TBR) of greater than one. The most researched fusion reactor designs are 'D' shaped tokamaks (also known as a conventional tokamak), but there has been an uptick of interest recently on spherical tokamaks, which have a smaller inner radius of the torus, and a smaller aspect ratio (of < 2.5)[5, 47].

Compared to a conventional tokamak, the spherical tokamak design has a unique tritium breeding challenge: to use the confined space between the inboard (IB) first-wall (FW) and central column magnet for breeding. The IB size is shrunk due to the compressed apple-shaped plasma core, reducing the volume space for tritium breeding. The role of the central column is to shield the magnet from high-energy neutrons and gamma rays. This displaces the volume to be used for any tritium breeding. This increases the demand on the outboard (OB) breeder blankets to produce a TBR > 1.2.

This study investigates a novel design approach for a spherical tokamak central column breeder design using high temperature materials that can act as a structure and radiation shield, enabling the use of potential sufficient radiation shielding performance whilst breeding tritium. This study also explores the trade-off between breeding in the central column and the resulting shielding performance.

This paper is organised as follows: the design philosophy is described in Section 2, the experimental methods used are detailed in Section 3, the results are presented in Section 4 with the discussion in Section 5, and a conclusion is provided in Section 6.

2. Design Philosophy

To design a breeder blanket within a spherical tokamak's IB components, there is a trade-off between volume dedicated for radiation shielding (from neutrons and gamma-rays) and space for breeding tritium. The philosophy for the approach is presented in the next subsections.

2.1. Design Process

A design process is initiated with two radial build designs for the central column of the tokamak. The intent is to produce two quasi 1D designs going through the thickness

*Corresponding author
**Principal corresponding author
mark.anderton@oxfordsigma.com (M. Anderton)
ORCID(s): 0000-0001-7047-0698 (C. Baus); 0000-0001-7419-3448 (R. Pearson); 0000-0001-8067-8732 (K. Mukai)

of the central column, from the plasma facing side to the centre. Each of the resulting designs would then be analysed and optimised for shielding and tritium production. With the goal of optimising for shielding and TBR, there are a number of key constraints and requirements on the concept designs:

1. The central column is required to have high-temperature superconducting (HTS) magnets of about 40 cm thickness, and a 15 cm thick steel vacuum vessel.
2. The plasma facing side of the design is required to be Tungsten armour with a thickness of at least 3 mm
3. The tungsten armour is subject to a radiative heat flux of 1 MW m^{-2}, in addition to bulk heating induced by the neutrons. These heat loads must be removed via a coolant. In addition, the heat flux into the cooled HTS magnets must be minimised while maintaining their low temperature
4. The design must include structural materials to hold the pressure of the coolant, as well as support the design as a whole.
5. The temperatures will vary through the thickness of the design, and the materials chosen must be suitable for the temperatures that they will experience.
6. All materials must be compatible with the neighbouring materials. This is particularly important in the case of liquid metal coolants, which can erode or cause corrosion on other materials.

Within these constraints and requirements, there is an opportunity to use materials for multiple purposes simultaneously, in order to maximise the use of space. For example, using a coolant which is also a breeder material potentially allows more breeding material to be included in the design. This helps to maximise TBR while also fulfilling the requirement to remove the heat loads. Similarly, using structural materials which also provide neutron shielding and/or a multiplying function also leaves more room for breeding materials for a given level of shielding performance.

Given these opportunities and constraints, there are key considerations and design choices to make in order to produce the concept designs. Firstly, a high temperature design is sought as it provides the potential for higher efficiency energy conversion, and enable the use of radiation shielding materials as structural components without the need for additional coolant channels, which potentially increases the space available for breeding and shielding. Accordingly, it is determined that the designs in this study will use only liquid metal breeders, as this provides the greatest density of lithium within the breeding zones.

2.1.1. Structural Materials

The aim of the central column breeder design is to enable high temperature (>600 °C) operation, thus, the materials selected should have suitable performance at these temperature windows.

Tungsten alloys and silicon carbide composite (SiC_f/SiC) have been selected due to their potential applicability for the aforementioned complex problems associated with an inboard breeding blanket for a spherical tokamak. Whilst traditional steels, such as stainless steel 316L have been identified as suitable for use in some components of a tokamak fusion reactor, they are limited by their low operating temperature of around 600 °C. The finalised set of structural materials considers radiation damage resistance and mechanical properties at temperatures beyond 1000 °C. Tungsten alloys and silicon carbide composite hold positive design characteristics for this application, where space is highly constrained, and performance requirements push beyond the boundary of what is possible with steels. The goal for this project and materials selection is to have a high reliability structural material, and it is considered that SiC_f/SiC and tungsten alloys that could be used enable high temperature operation by acting as a structural material (and shielding material).

Tungsten Alloys Any breeder blanket design in the central column that uses radiation shielding as both the shield and structural material is a novel idea. Alloying tungsten (W) with rhenium (Re) - 9 wt% to 25 wt% - has shown to improve ductility and manufacturability [41]. This could enable W-based alloys to function as both a shielding and structural material [25] thus providing an efficient way of making use of space within compact regions. This type of alloy is highly dense, has good radiation shielding properties (mainly a resultant of W), high gamma shielding performance, and has a good operational temperature window. As a result, the use of W-Re as a dual-purpose shielding and structural material could allow for a reduction in the thickness of the vacuum vessel and a greater breeding space and operate at higher temperatures than normal structural materials (i.e. steels). Preliminary data suggests that tungsten and FLiBe are compatible, under high temperatures [32]. Combining this with boron (as tungsten boride), potentially enriched in boron-10 which has a very high neutron cross section, at the most in-board section of the shield would provide good neutron absorption characteristics [3, 53].

W-Re alloys have been shown to be somewhat resistant to liquid lithium corrosion at 1371 °C [29]; the degree at how resistant these alloys are is beyond the scope, but further work is needed. The phase diagram for the material system can be found in Fig. 1 which demonstrates that the sigma phase forms at approximately 27 wt% Re. Sigma phase is known to embrittle Tungsten materials [40]. The W-24.5Re-2HfC alloy system is a promising candidate as the alloy system has the following properties:

1. Previously studied in the 1960s-80s for high temperature applications [25, 40]
2. High recrystallization temperature (∼1700 °C) [20].
3. Improvement in strength at high temperatures [26].
4. Better Ductile-to-brittle transition temperature (DBTT) compared to W [26].
5. Possibly better radiation damage resistance compared to W due to increased radiation recombination zones (due to HfC precipitates).
6. Hf could produce intermediate level waste [27].

7. Hf is a good neutron absorber. The HfC particles form nano-sized (~50 to 150 nm) precipitates within the matrix that stabilise the W-Re matrix. This can be seen in the increase in recrystallisation temperature and reduction in DBTT in Fig. 2.

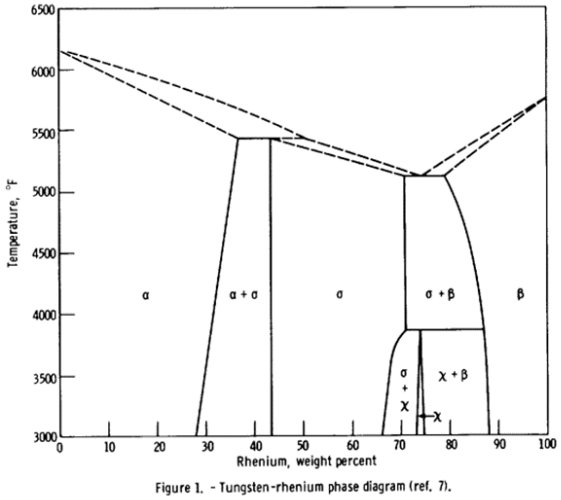

Figure 1: Phase diagram of W-Re alloy system. Reproduced from [40]

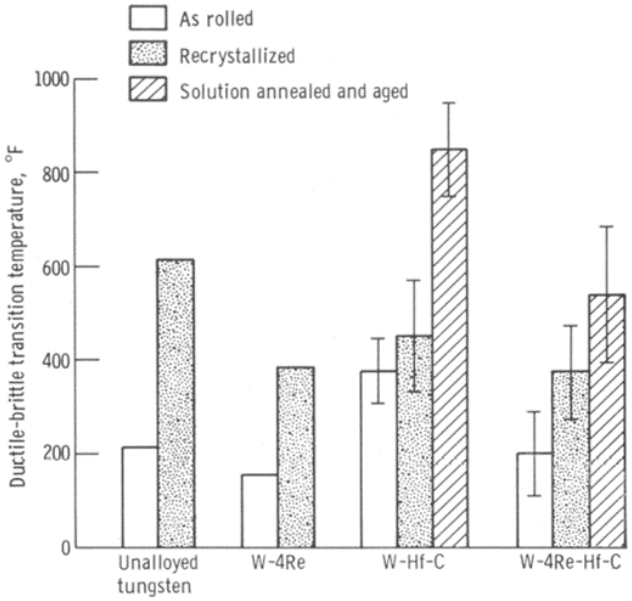

Figure 2: Recrystallisation temperature of various W alloy systems. Reproduced from [20]

SiC_f/SiC SiC_f/SiC consists typically of a SiC matrix with SiC fibres embedded in the matrix to improve structural properties compared to monolithic SiC, which as a pure ceramic is brittle. SiC_f/SiC is now seeing greatly increased use in the aerospace industry due to its strong heat resistance and toughness. Recently, nuclear-grade SiC_f/SiC has been used as fuel cladding for fusion reactors [7], where shorter tube pieces were joined to form the long tubes required for the cladding.

In recent years many advances have also been made in the manufacturing of SiC_f/SiC into complex shapes [23]. Consequently, the interest for fusion application has picked up and designs for blanket, divertor, and first walls based on SiC_f/SiC have been created [38, 48]. Several properties are favourable for such conditions. SiC_f/SiC is thermomechanically stable up to more than 1000°C and serves as an electrical insulator. Together with its good compatibility with LiPb [37] and its expected performance in reducing the effects of MHD, it is being considered as both a structural and functional material for advanced breeder blankets (see Section 2.1.2).

It has been demonstrated that SiC_f/SiC has very good performance under neutron irradiation, a property important if used as structural material in the blanket or in the central column design discussed herein. Nuclear-grade SiC_f/SiC has been tested up to approximately 100 dpa [17, 22]. So far, no irradiation with neutrons at fusion energies (14.1 MeV) at high temperatures has been performed. As with other structural materials, some uncertainties remain about such neutron irradiation. The swelling behaviour is reasonably well contained under the irradiation tested as the material saturates quickly [17].

The thermal conductivity of SiC_f/SiC is important for the IB breeding design. It is low at 20 $W\,m^{-1}\,K^{-1}$ and under neutron irradiation quickly drops to about 5 to 7 $W\,m^{-1}\,K^{-1}$ [8, 18]. This is important, as for large wall thicknesses heat removal by the coolant is insufficient, pushing the design space of the first wall and other temperatures to their limit for the case of central column usage (see Section 3.1).

Several improvements to the thermal conductivity by doping SiC_f/SiC are currently being pursued but even though they are expected, positive results have not yet been published.

SiC_f/SiC and tungsten have similar thermal expansion rates (W: $4.3 \times 10^{-6}\,K^{-1}$, SiC_f/SiC: 4 to $4.5 \times 10^{-6}\,K^{-1}$) and, as such, their compatibility is expected to be good. Their thermomechanical stability under neutron irradiation was found to be good as well [46]. In combination with tungsten, SiC_f/SiC could serve as a first wall candidate, even when only a thin layer is applied in powder form to prevent sputtering effects.

Tritium permeation of SiC_f/SiC is much better than for steels. The permeation coefficient of monolithic SiC is about 4 orders of magnitude lower compared to SS316 [54] and SiC_f/SiC can also be orders of magnitudes less permeative [16]. Therefore tritium can be contained within the breeding material and will not contaminate secondary coolants or other materials in the vacuum vessel.

Manufacturability remains as one of the most important challenges for SiC_f/SiC [38]. To create complex coolant channel shapes, further R&D is needed. Simple channel shapes and piping are deemed possible with the latest prepreg sheet-based processes.

Overview Following the review of materials, the two leading candidates for structural materials were tungsten-based alloys, and SiC_f/SiC. Tungsten-based alloys offer good shielding performance, which may be advantageous in the confined space of the central column, but equally may (or may not) inhibit breeding when in front of the breeder/coolant. SiC_f/SiC offers good structural performance, but has the opposite effect on neutronics as they are essentially transparent to neutrons, which is expected to be beneficial for breeding. These two options then neatly bound the design space for structural materials.

2.1.2. Breeder Materials

The choice of breeder material dominates the neutronic characteristics of the blanket and its resultant tritium breeding capability [10]. Liquid breeder concepts have long been considered the most promising for commercial fusion and offer several benefits over solid breeding material. There are no issues associated with neutron damage for the breeder itself, nuclear heating is deposited directly into the breeding material, and tritium can be extracted and breeder refilled while the system is online. A liquid breeding material can also serve as the coolant, either partially or fully replacing it and thus reducing system complexity. These characteristics allow the blanket design to be simplified.

For the IB side, size limitations and the practical design considerations, self-cooled single-fluid designs have been down-selected for the initial scoping exercise. These will be referred to as self-cooled (SC) designs. Specifically, pure lithium and lithium lead have been selected as candidate SC blanket materials. Tritium is bred and retained in the liquid, which flows through the blanket cooling channels to a heat exchanger outside of the vacuum vessel. It is assumed that there is no tritium permeation into the surrounding structural materials. Here, outside of the high flux neutron environment, a tritium recovery system can be employed to extract the bred tritium [33].

The use of liquid metals does introduce issues, including ones associated with magneto-hydrodynamics (MHD) which can lead to severe pressure drops. Liquid metals require high velocity pumping. Therefore, there are associated parasitic loads incurred and steps, such as the use of insulating materials, should be taken to avoid MHD effects [33] [15]. These will be discussed in Section 5.

Lithium occurs naturally in a 7.59 % Li-6, and 92.41 % Li-7 ratio [43]. The enrichment of the Li-6 isotope can dramatically affect the breeding performance. Both isotopes are capable of producing tritium following neutron capture. At higher neutron energies the Li-7(n,n'α)T reaction presents a better cross-section performance. The Li-7(n,n'α)T interaction has the benefit of scattering the neuron rather than absorbing it and will produce tritium without reducing the neutron population. Enriching Li-6 for the breeding material can result in an increase in TBR, but because it strongly depends on the energy spectrum at the beginning of the breeder material and the change of the spectrum with depth in the central column, the effect is best studied in numerical simulations. Typically several different enrichment levels ranging from natural Li-6 to 100 % enrichment are simulated and the TBR analysed as a function of enrichment.

A significant materials challenge presents itself in lithium self-cooled blankets operating at elevated temperatures on the order of 700°C. Pure lithium is known to be corrosive [36, 55]. On interaction with steel, for example, the reaction can occur via transgranular or intergranular mechanisms. Transgranular corrosion usually occurs at higher temperatures and lower non-metal impurities through a dissolution, mass transfer mechanism. Intergranular corrosion is strongly dependent on the carbon and nitrogen presence [1, 24, 31, 55]. Consideration should be taken to remove these impurities to reduce overall corrosion issues, or the material compatibility should be chosen to optimise for this design choice [33]. Coatings have been a significant area of research since they act to decouple the liquid metal and structure to increase performance, but they also increase design complexity [1, 39]. Vanadium structural material has been identified as a candidate material that is potentially compatible with lithium coolant, but still has issues with embrittlement by oxygen, hydrogen and other environmental contaminants [1, 34, 39].

Adding lead to liquid lithium reduces the activity coefficient [11] and increases compatibility with many materials. The lithium-lead (LiPb) SC design typically uses LiPb at concentrations of 17 at% Li and 83 at% Pb for which the two metals form a eutectic alloy at 508 K [19]. LiPb acts as both a breeding material and a neutron multiplier achieving reasonably high TBR values and has therefore been employed in several well-established designs such as the Dual Coolant Lithium-Lead (DCLL), and also the Helium Cooled Lithium-Lead (HCLL) progressed for ITER [10]). The neutronics of LiPb is highly governed by the performance of Pb, which has high neutron scattering power but low neutron moderation power. For a sufficiently high TBR, a characteristically large blanket zone is typically required. This is due to the Li-6 breeding reaction efficacy being higher for lower neutron energies [10]. Enrichment values as high as 90 at% might be needed for LiPb blanket systems [14].

LiPb is found to be compatible with ferritic steel and SiC_f/SiC and can facilitate higher temperatures to maximise thermal power cycle efficiencies [38]. As previously noted, in combination with SiC_f/SiC or similarly compatible electrically insulating materials, the MHD effects of LiPb are expected to be reduced [15].

2.1.3. Neutron Multiplier Material

In the confined space of the central column, it is not clear whether a multiplier would improve tritium breeding by multiplying neutrons, or reduce overall TBR by taking space that could otherwise be used for breeding. This effect is investigated in the concept designs.

Lead is a credible multiplier material and may be alloyed allowing it to operate as a liquid or a solid neutron multiplier, depending on alloy material. [12] provide a detailed

breakdown of potential options. In addition to this, lithium-lead alloy has the advantage of combining tritium breeding capability and multiplication into a single material and can be used in liquid form.

Beryllium is a valuable alternative to lead, offering neutron multiplication properties similar to lead, but far lower parasitic absorption, at the neutron energy spectra expected in the scale of the DEMOnstration power plant (DEMO) [12]. Optimal performance, however, requires very high beryllium to breeder volume ratios [10]. There is thus a trade-off between breeding efficiency and space utilisation. Despite this, a smaller volume breeding zone is possible, compared to lithium-lead, for comparable breeding rates. Due to its superior neutron breeding capabilities, beryllium, then, would seem a preferable option for inboard breeding, at least from a volume utilisation perspective.

Beryllium has some significant disadvantages though when compared to lead as a multiplier material. Its thermal properties indicate that it is unsuitable for use in a liquid metal blanket, in contrast to lithium-lead, which can be liquefied for use as both breeder and coolant. Cooling efficiency is thus limited by beryllium's thermal conductivity, limiting its potential locations in the blanket [15]. This means that additional cooling is required, at a cost of both space within the reactor blanket for coolant channels, and outside the reactor where coolant feeds will reside. Conversely, the requirement to retain the solid phase for beryllium will limit the operational temperature of the reactor, and thus its potential use cases. For this reason, it is worth considering alloying options for beryllium in order to improve its operational temperature range [12]. It is further important to note that the availability of beryllium is very limited. In fact, the current global annual supply would not fulfil the amount required for a single DEMO reactor [15, 35]. Production would need to be increased significantly.

Beryllium is also reactive with pure lithium. One proposed DEMO blanket, the Helium Cooled Pebble Bed (HCPB) utilises lithium-based ceramic and beryllium pebbles within a structural matrix [10, 15]. Whilst this does not necessitate separation of lithium and beryllium, it does not offer the advantages of self-cooling lithium-lead blankets. Maintenance requires removal of the blanket modules [10] and this access would be required in a confined region were such a design to be used inboard of the reactor.

We have considered how it might be possible to utilise beryllium as a multiplier in an inboard blanket. The aforementioned reactivity of lithium and beryllium means that the two materials need to be contained and isolated from one another. One possible solution is a 'Smarties tube' approach. In such an approach, the blanket would contain built-in tubes in which beryllium pebbles would reside. This would facilitate access to allow beryllium to be refreshed over time. This concept is illustrated in Fig. 2.1.3.

The multiplier tube design and material would need some consideration. The lithium compatibility, neutron-transparency and thermal properties would be paramount. Whilst it would be expected that the tubes themselves would not be structural, it would be advantageous to be able to pressurise the tubes themselves with a purge gas. This would allow harvesting of the tritium yielded by the neutron multiplication reactions from the beryllium [44].

It should be noted that this design significantly increases the complexity of the blanket. The inclusion of a purge gas would increase the complexities of the manifold design for coolant and purge gas inlets and outlets. Once again, this begs the question of whether such an approach is attractive, or even feasible, for inboard breeding. It may be that such a system presents valuable characteristics for outboard breeding, but because compromises would have to be made on the inboard side, essentially sacrificing breeding efficiency for the practicalities of reactor operation and maintenance, it would be unsuitable for inboard.

A beryllium titanate ($Be_{12}Ti$) material was chosen as a multiplier for the Li-concept. The multiplier is allowed to vary in size from zero to a significant proportion of the thickness, and also vary in location within the breeding section from front to back, as it is not clear whether the multiplier material is more beneficial than the same volume of additional breeder, and if so, where the optimal placement is. It should also be noted that the multiplier must not be right at the front of the breeding/cooling channel without active cooling, as the first few centimetres of coolant are vital to carry heat away from the plasma facing wall.

The multiplier would most likely take the form of a pebble bed within a thin channel structure, with a helium purge gas, as beryllium also produces tritium.

2.1.4. Radiation Shielding Material

High thermal and fast neutron cross-section provides good absorption characteristics. Tungsten borides offer an excellent combination of neutron absorption, neutron moderation (through the W(n,2n) reaction), gamma-ray attenuation, and density, and have been shown to offer an order of magnitude level of performance to in-board neutron shields, especially tungsten (penta)boride [52].

The shield materials chosen as part of both concepts are W_2B, W_2B_5, WB_4 and WB_2. They are intended to carry their own self weight (only) without imposing a load on the nearby structure. Therefore, cracking can likely be tolerated so long as it does not impair other functionality or begin to provide a thermal path to the vacuum vessel. They are therefore capable of operating across a large range of temperatures, proving flexibility in the design. The thickness of shield material is allowed to vary within the limits of the overall thickness and depending on the other thicknesses specified, in order to optimise the trade-off between shielding and TBR.

2.1.5. Vacuum Gap

A 1 cm vacuum gap is specified between the rear of the shield and the vacuum vessel. This is to thermally isolate the vacuum vessel from the high temperature shielding/breeding assembly, allowing only radiation to transfer the heat. The gap also structurally isolates the two assemblies, so as not

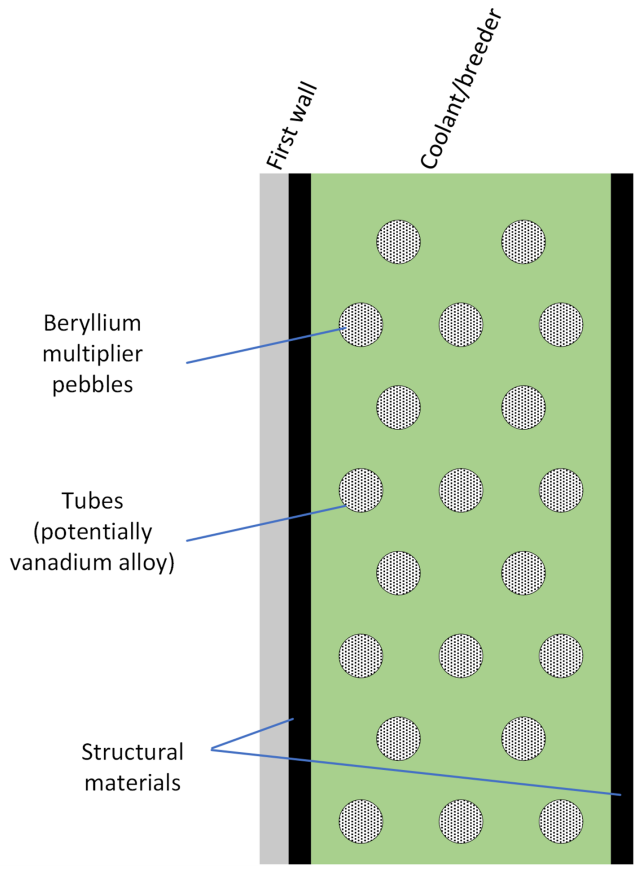

Figure 3: Radial build 'Smarties tube' concept blanket. The design is shown in a cross-section plan view. Note: elements are not to scale.

to impose stresses on the vacuum vessel or shield due to mismatch in temperatures and thermal expansion.

2.2. Overview of Concepts

Since the geometry of a tokamak's central column varies depending on the design, the decision was made to fix certain parts of the geometry to values reasonable for a large spherical tokamak as follows:

1. Total length of 100 cm
2. HTS magnet length fixed at 40 cm
3. Vacuum vessel length fixed at 15 cm
4. Tungsten first wall armour length fixed at 3 mm

The remaining 44.7 cm of space is left to optimise for shielding and tritium breeding. Guided by these design decisions, options, and constraints mentioned previously, two concept designs were produced for the radial build of the central column to explore the design space and the potential ability to breed tritium. These two concepts are demonstrated in Fig. 2.2.2. Each contain variables such as thicknesses of breeder/coolant material that were then optimised in the analysis phase of the project.

As mentioned previously, each concept has two "structure" sections and a vacuum gap of 1 cm, all of which are fixed in length. These sections will be subtracted from the remaining optimisation space. Since the length of both structural sections was decided to be less than one centimetre, the remaining an additional length was added to the shielding section in both concepts to increase this length to an integer value and the subtracted from the concept's optimisation space.

Both concepts use 3 mm of tungsten armour which is supported by a 3 mm W-24.5Re-2HfC structure for the Li-concept and a 2 mm SiC_f/SiC structure for LiPb-concept. The Li-concept will use pure lithium as a breeding material whereas the LiPb-concept will use lead-lithium with the ratio of lead:lithium at 83:17. Both concepts consider lithium-6 enrichment at natural 15 %, 30 %, 45 %, 60 % and 90 % levels. The Li-concept will use $Be_{12}Ti$ as a multiplier and the LiPb-concept will use the lead in the lead-lithium breeding material as its multiplier. Both concepts will consider WB, W_2B, W_2B_5 and WB_4 as shielding materials. As noted previously, initial structural and thermal analysis conducted concluded that both concepts will require a vacuum gap between the shield and the vacuum vessel, in order to limit the heat flux from the high temperature shield/breeder section into the vacuum vessel and ultimately the HTS coils. The following sub-sections discuss the reasoning between the design details included in this concept.

2.2.1. High Temperature Design 1 - W-Re-HfC and Li Based

Liquid lithium is chosen as the coolant and breeder material for the Li-Concept. It offers the chance to maximise TBR in the confined environment of the central column, and also has good heat transfer properties and requires low pumping power. The thickness and required flow rate are variables within the concept design, and the effects of enrichment level is also investigated in the analysis. A coolant temperature of 1000 K was chosen for the Li-concept.

The structural material provides pressure containment for the liquid lithium coolant. Two tungsten alloys are taken forwards as part of the Li-concept (W-25Re and W-24.5Re-2HfC) and investigated in the analysis. Both alloys exhibit good corrosion resistance to liquid Lithium below temperatures of 1371 °C, and otherwise offer good or reasonable structural properties up to temperatures of 1200/1300 °C for W-25Re and 1700 °C for W-24.5Re-2HfC. They offer the ability to provide some shielding as well, thereby maximising use of space. A maximum surface temperature of around 1200 °C was specified for Li-concept. An alternative structural material of SiC_f/SiC was not taken forward for the Li-concept, as it suffers more from corrosion challenges with liquid lithium, albeit that with a coating its use may be possible. A thickness of 3mm was chosen as discussed in Section 3.2.

2.2.2. High Temperature Design 2 - SiC_f/SiC LiPb Based

A silicon carbide composite structural material was chosen for the LiPb-concept, to provide pressure containment

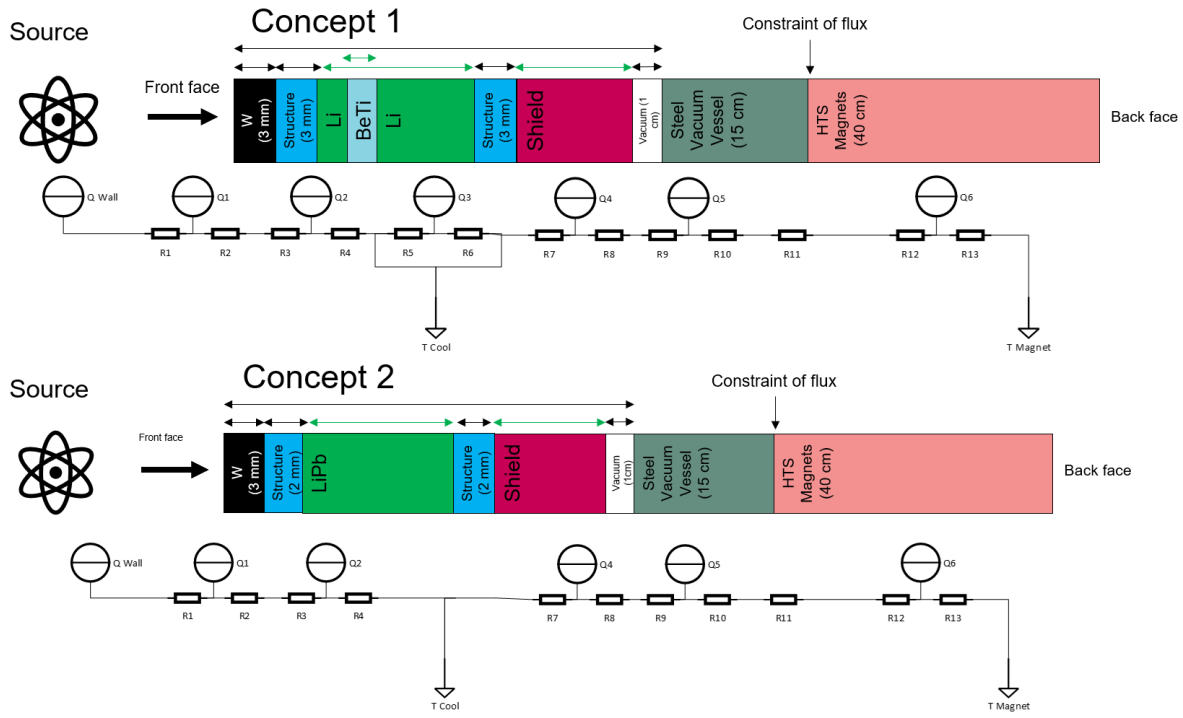

Figure 4: Overview of concepts 1 (L1) and 2 (LiPb) radial build geometries and thermal networks. Black arrows represent a fixed space, green arrows represent a variable space.

for the coolant and support the first wall armour. The material provides no shielding and is essentially transparent to neutrons, maximising the ability to produce tritium but potentially at the expense of shielding. It retains good material properties at high temperatures, but has poorer thermal conductivity than the tungsten alloys in the Li-concept. Therefore, a reduced thickness of 2 mm was chosen to keep the first wall temperatures within reasonable limits, as discussed in Section 3.2.

A liquid lithium-lead coolant was chosen for the LiPb-concept, to explore the use of an alternative breeder material with a potentially higher technology readiness level. The coolant offers good heat transfer properties, works as a breeder material, has better compatibility with potential structural materials, and also contains lead, which can act as a multiplier. The thickness of coolant channel and required flow rate were allowed to vary in the LiPb-concept, as well as the Lithium enrichment level. A coolant temperature of 1000 K was chosen for the the LiPb-concept design.

3. Experimental Method

3.1. Thermal Analysis

The method chosen aims to determine that the materials operate within their limits and sufficient cooling power is provided for these designs.

A thermal network model has been developed for the designs respectively to understand steady state temperatures. The thermal network is solved by applying an electrical analogy to the heat transfer problem. Kirchhoff's laws can be re-stated as: The heat flow at a node must sum to zero and the temperature difference around a loop must sum to zero.

Conduction resistances can then be defined as:

$$R_{\text{conduction}} = l/kA \tag{1}$$

where l is the thickness of the conductive component, k is the material thermal conductivity and A is the surface area through which the heat flux acts. The current inboard breeder is considered in a radial sense, and is assumed uniform throughout a height of 15 m. Therefore, appropriate areas are considered for the front and rear faces of each component.

Similarly, convection resistances can be defined as:

$$R_{\text{convection}} = 1/hA \tag{2}$$

Where h is the convection heat transfer coefficient and A is the surface area through which the heat flux acts. The heat transfer coefficient has been taken from previous work for the outboard blankets [6] which used a Lithium coolant. Correlation data for liquid metal heat transfer coefficients is not readily available, however, best practice [13, 51] was used to generate a scaled CFD model to calculate achievable heat transfer coefficient.

Finally, surface to surface radiation heat flow, q, between two cylinders can be calculated as:

$$q = \frac{\left(\sigma A_1 \left({T_1}^4 - {T_2}^4\right)\right)}{\left(1/\epsilon_1 + \left(1-\epsilon_2\right)/\epsilon_2 \left(r_1/r_2\right)\right)} \tag{3}$$

Where subscript 1 and 2 refer to the smaller and larger radius cylinders respectively, σ is the Stefan-Boltzmann constant, ϵ is the material emissivity, r is radius, A is surface area and T is temperature. A heat flux of $1\,\mathrm{MW\,m^{-2}}$ is applied over the first wall area as a current source.

The maximum outlet temperature is selected representing the extreme operating condition of the column, and will lead to maximum structural temperatures predicted in the thermal network. This can then be compared to allowable temperatures to check the constraints have been achieved. It is a pessimistic design point to select, as this condition only occurs at the outlet to the column. A maximum surface temperature of the HTS magnets of 40 °C is applied at the other end of the network. The heat flow at this location can then be checked with the magnet specification for acceptability. Volumetric heat fluxes from representative neutronics assessments are added for each component. For the vacuum vessel, this heat flux can be made negative to account for a vacuum vessel cooling system, if required.

The layout of the concepts is shown with the corresponding thermal network in Fig. 2.2.2.

The components are represented within the thermal network in Fig. 2.2.2 as follows:

- First wall heat flux – Q Wall = $1\,\mathrm{MW\,m^{-2}}$.
- Tungsten armour – Conduction resistances R1 and R2, representative of half the armour thickness each.
- Tungsten armour neutronic heating – Q1.
- First structural wall - Conduction resistances R3 and R4, representative of half the structure thickness each.
- First structural wall neutronic heating – Q2.
- First structure to coolant – Convective resistance R14.
- Coolant to multiplier – Convective resistance R15.
- Multiplier - Conduction resistances R5 and R6, representative of half the multiplier thickness each.
- Multiplier neutronic heating – Q3.
- Multiplier to coolant – Convective resistance R16.
- Coolant to second structure – Convective resistance R17.
- Second structural wall - Conduction resistances R7 and R8, representative of half the structure thickness each.
- Second structural wall neutronic heating – Q4.
- Shield - Conduction resistances R9 and R10, representative of half the shield thickness each.
- Shield neutronic heating – Q5.
- Vacuum gap – Cylindrical surface to surface radiation resistance R11.
- Vacuum vessel - Conduction resistances R12 and R13, representative of half the vessel thickness each.
- Vacuum vessel neutronic heating – Q6.
- Coolant temperature – T Cool = 1000 K for high temperature design.
- HTS magnet temperature – T Magnet = 313 K.

The same naming conventions for components has been used for the LiPb-concept, and therefore the network is similar to the Li-concept with the removal of components that relate to the multiplier (Q3, R15, R5, R6, R16). The remaining resistances are re-calculated using material and geometry data applicable to the LiPb-concept, including volumetric heat fluxes from representative neutronics analyses, before the network is solved.

3.2. Structural Analysis

For this concept level analysis, simple calculations can be made to ensure that sufficient thicknesses of structural materials are provided to withstand the primary loading of the pressure of the coolant on the structure. A simple pressure vessel calculation can be made assuming a cylindrical column,

$$\sigma = (Pr)/t \tag{4}$$

where radius equal to r, containing a pressure of P for a given thickness t.

3.3. Neutronics Analysis

The tritium breeding and radiation shielding performance is determined by using neutronic simulations. Monte Carlo N-Particle (MCNP) Version 6.2 was used in this study with the TENDL2019 [21] nuclear cross-section database was used. A neutron source "175 ITER-DT" [50] was used because it provided a representation of the expected flux on the first wall's tungsten armour. As a result, the line will tend higher in the thermal and epithermal range since more neutrons are recorded per bin. The same binning scheme for the neutron source was used as the flux binning tallies. The number of particles simulated was selected to be 10^5 neutrons per simulation in this study due to the large computation time required for all runs. However, a select few models were chosen to be re-run with the more common 10^8 neutrons per simulation.

3.3.1. Geometry

The quasi 1 dimensional geometry of the breeder blanket used here was optimised to minimise computational time to ensure a large parameter sweep could be conducted within the project time.

The model was based on a series of cylinders of radius 30 cm with a length of 1 cm, forming a disc shape. Since each disc is of equal surface area and are arranged sequentially, combining all the discs can be considered a cylinder which would have the same length as the distance from the first wall to the end of the HTS. Therefore, a complete cylinder

acts a representation of a cut out from a region of the central column from the first wall armour all the way through to the HTS magnets.

This larger cylinder was then wrapped in a 'bounding box' of a homogeneous mix of 80% 316L-ITER Grade stainless steel and 20 % water (H_20) with a wall thickness of 20 cm to represent pipework and surrounding machine structure. This was chosen to provide a region of material which will scatter and/or absorb neutrons as a surrogate for the surrounding materials in a real tokamak fusion reactor.

A vacuum of radius 30 cm and length 5cm was placed at front of the first disc and surrounded by the bounding box. For the purposes of this report, the cylinder which is formed because of the series of discs, bounding box and vacuum will be referred to as a 'canister geometry'. A second vacuum of radius 30 cm and length 5 cm was then placed outside of the canister to house the neutron source. The intention behind having these two vacuums was to allow the source to be unperturbed initially when neutrons are generated and to allow any neutrons that are reflected by the first few discs to potentially be reflected back by the bounding box surrounding the vacuum inside the canister.

The majority of the material arrangements in both concepts have a length greater than 1cm. Such material arrangement are split into 1cm wide sections so that the neutron and photon flux can be measured at the start and end of each disc to measure how it is transformed through the material. Any remaining section that has a length of less than 1cm will not be split and added with its true length.

An example plot from the MCNP plotter illustrating the splitting can be seen in Fig. 3.3.1 for Li-Concept and Fig. 3.3.1 for the LiPb-concept.

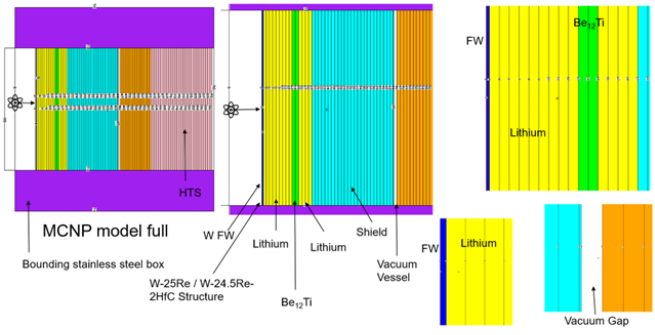

Figure 5: Two-dimensional MCNP renderings for an example geometry for Li-concept

3.3.2. Optimisation Space and Geometry Permutations

The approach was taken by where a list of all possible permutations for each concept was generated and each permutation was run as an independent MCNP simulation. The number of permutations observed in the Li-concept (43,740) is significantly higher than that of the LiPb-concept (1,920) due to the greater geometry complexity by the inclusion of the multiplier. The permutations considered in the LiPb-concept only consist of the materials in question for the shield material, lithium-6 enrichment levels and their

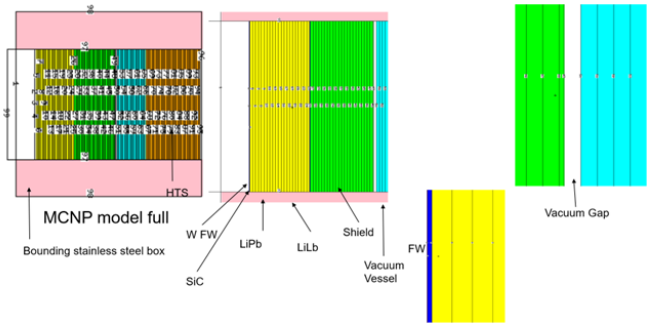

Figure 6: Two-dimensional MCNP renderings for an example geometry for LiPb-concept

lengths. In comparison the number permutations required for the Li-concept are the same as for the LiPb-concept with the inclusion of structural material choice, multiplier thickness and multiplier position compared to the first wall's structure. The effect of varying the length of both breeding sections was implemented to vary the multiplier's position with respect to the shield to determine whether the breeding would be improved with the multiplier closer to the first wall or closer to the shield.

This approach was taken because there is a complex relationship between the choices of materials and their associated sizes and positions with respect to each other. Therefore, this approach enables the opportunity to accurately measure changes in the neutron flux at different points in the geometry and compare changes in the neutron flux as a result of changes in materials, material thicknesses or material positions. This is illustrated by Fig. 3.3.2 which provides an example of how the neutron flux spectrum changes with an increase in the thickness of a tungsten boride (WB) shield. As a result, this allows for optimisation of the radiation shield (to reduce the neutron flux at the HTS surface) and maximize TBR.

To reduce the number of permutations required for the Li-concept, the length of both breeding sections was limited to a minimum of 2 cm with increasing in 2 cm increments. The length of the multiplier was limited to a maximum of 10 cm from a minimum of 0 cm increasing in 2 cm increments. Finally, the length of the shielding section was limited to 6.1 cm with increasing in 2 cm increments. Although increasing the length of each section in 1 cm increments would have been preferred, the time taken to compute twice as many permutations was perceived to be too great for the project time. Since trends have already been derived with the current results, additional studies could be carried out with a reduce increment size in future based on a reduced geometry range.

For the LiPb-concept all permutations were considered from a minimum breeding length of 0 cm to a maximum breeding length of 39 cm, a minimum shield length of 4.3 cm to a maximum shield length of 43.3 cm. Here each change in the geometry's scale resulted in a 1cm increase in the length of the breeder and a 1cm decrease in the length of the shield.

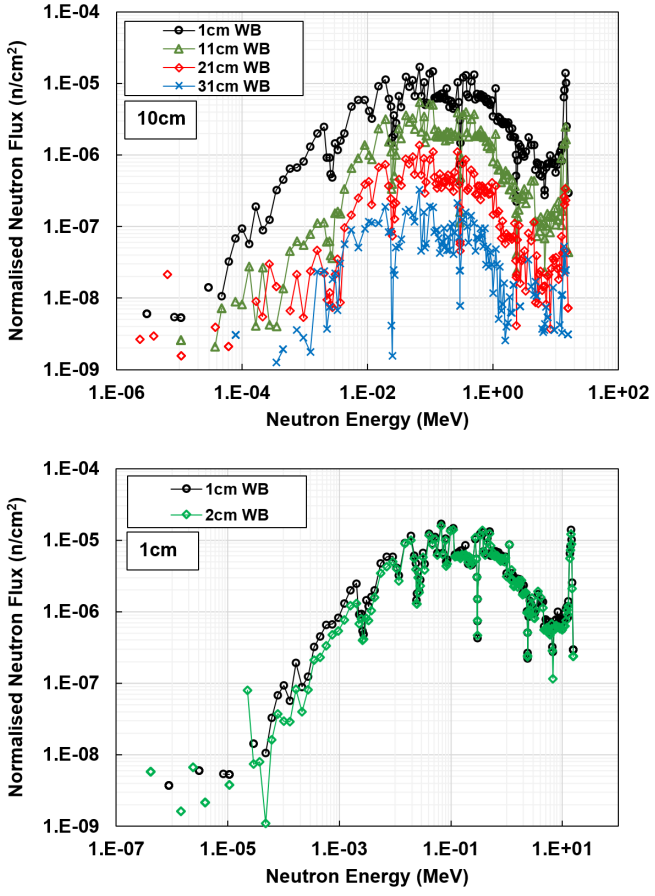

Figure 7: Changes in neutron flux spectrum in 1 cm and 10 cm regions of a tungsten boride (WB) shield.

3.3.3. Tritium Breeding Ratio

The MCNP FM multiplier with a reaction type of 105 for tritium production from Li-6 and FM multiplier with a reaction type of 205 for tritium production from Li-6 and Li-7.

It should be noted that while overall TBR of a the tokamak must be greater than unity, it is not expected that this will be at all possible in the central column. We therefore distinguish between three different TBR values: the local TBR (assuming full coverage), global TBR_{IB} (taking geometry into account but limited to the breeding of the inboard system) and global TBR_{IB+OB} (including both inboard and outboard systems). Any breeding which takes place on the inboard side will contribute positively to the global TBR_{IB+OB}. Optimisation is obtained from studying the local TBR and the highest local TBR designs are taken forward to calculate the global TBR values for a spherical tokamak design.

3.3.4. Model Limitations

The main sources of limitations for the neutronics model are as follows:

1. Simple geometry space
2. Fusion neutron source had a disc shape that does not an accurate representation of the neutron flux profile found across the entire central column.
3. Neutron interactions with surrounding components was simulated with the steel bounding box.

It should be noted that the aforementioned limitations indicate that the results need to be interpreted with the following considerations:

- The TBR readings are local to the model.
- The model has been designed with the maximum breeding space possible. Here, no components which are commonly found inside breeding models such as pipes and tubes are not considered. The introduction of these components would reduce the TBR since less of the breeding volume would be occupied with lithium.
- The model is designed around a section in the middle of the central column which tends to have the most significant neutron flux and has the largest geometry space, therefore, will likely always have the highest TBR of the entire central column.
- The neutron flux values are from a normalised source, therefore, the source requires an appropriate weighting factor to be relevant to a full power year and geometry fraction.

However, it should be said that the model setup was designed for fast computational time to analyse tens of thousands of simulations in a short time. This fast prototyping can be very effective at determining a first-pass principle to engineering design.

3.3.5. Validation and Systematic Uncertainties

Both concepts were cross-checked for a fixed design of 20 cm breeder and WB_4 as shielding at all available enrichment levels. For this, a different Monte Carlo code (OpenMC [42]) with two cross-section libraries (TENDL2019 and ENDF/B-VII.1 [4]) were compared to the results obtained with above described default simulation (MCNP + TENDL2019). Using OpenMC + TENDL2019 resulted in an around 5 % increase over OpenMC + ENDF/B-VII.1. However, the comparison of MCNP + TENDL2019 resulted in a enrichment-dependent underestimation by OpenMC + TENDL2019 by about 34 to 9 % with decreasing differences for higher enrichment, which could be attributed to small differences in the geometric description between OpenMC and MCNP. In either case, this uncertainty has little influence on the optimisation strategy for finding the optimal design with high TBR. When calculating a global TBR for a specific reactor design.

4. Results

The different designs were analysed in a multidimensional manner. Of interest are the shielding properties after

the vacuum vessel (VV) and at the beginning of the HTS magnet in terms of total neutron flux, fast neutron flux, photon flux and the TBR. Good designs have been selected by requiring a lower than the benchmark total and fast neutron flux and a high TBR. Lower photon fluxes than than the benchmark flux are also preferential. However, this criteria was not considered in the selection based on the assumption that it has less impact on the magnet lifetime.

A Pareto curve, which describes the incremental changes of the TBR value due to changes in the shielding performance, was derived from the simulation data. The Pareto curve envelopes the data on the high TBR side of the distribution and shows the maximum achievable TBR given a certain shielding performance. With it, the trade-off can be quantified. It should be noted that, as it envelopes the simulation results, it represents a breeding-optimised result which does not consider economic factors (e.g., significant additional costs associated with enriching lithium).

All characteristics depend on several parameters including the positions and thicknesses of breeder layers, the enrichment level of the lithium in the breeder and the thickness of the multiplier. Therefore, not all dimensions can be plotted at once to compare and derive a best design. An approach was chosen to show an overview of shielding performance against TBR for all simulated designs. This was then examined in more detail to understand how different parameters influence the validity of a design. Finally, a design window was selected that provides slightly improved shielding performance compared to the benchmark and maximises TBR.

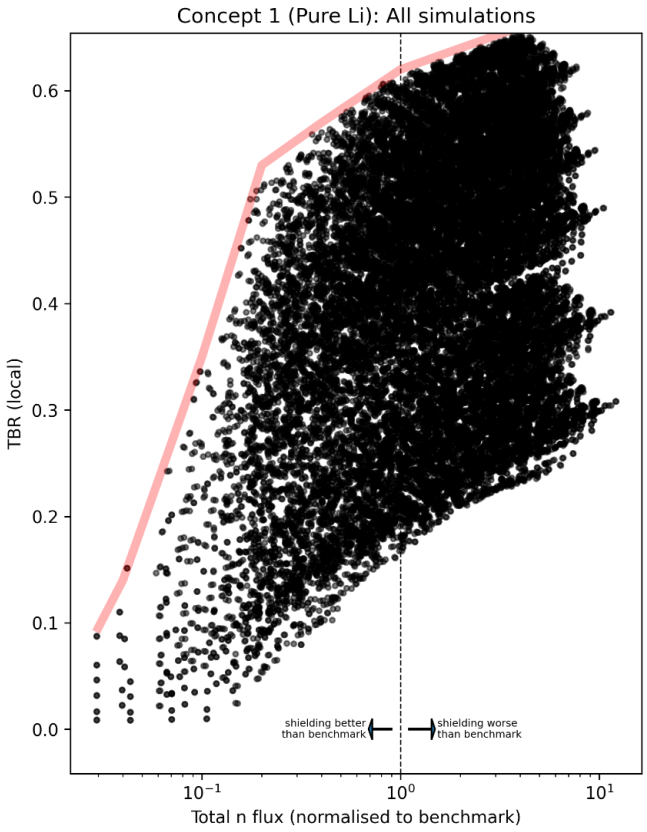

Figure 8: Local TBR vs total neutron flux after the VV and at the beginning of the HTS magnet for all designs of the Li-concept. The red curve indicates the Pareto curve.

4.1. Li-concept

The Pareto curve enveloping all designs of the Li-concept can be seen in Figure 8. A local TBR of slightly above 0.6 can be reached at the total neutron shielding performance of the benchmark shield. The neutron flux can be decreased by almost 2 orders of magnitude but at a factor of 6 in TBR because the breeder space is taken up by the shield. Sacrificing some shielding performance compared to the benchmark to gain a higher TBR is not recommended because the local TBR does not reach 0.7 in any design. Depending on the positions and enrichment levels a wide range of TBR values are observed in the simulation data.

Dividing the dataset into enrichment levels and removing the multiplier layer reveals distinct trajectories of TBR vs flux (cf. Figure 4.1). A higher enrichment has a higher TBR, which is a result that was not anticipated before the simulations were performed. Usually pure lithium designs have a maximum TBR between 30 and 70 % depending heavily on the thickness of the breeder. There are minor differences between the shielding types. The best performing materials are ones with high boron content as found in the initial scoping study.

Figure 4.1 shows, for a fixed breeder thickness, shielding and structural material, the TBR and neutron flux against enrichment. With higher enrichment the TBR is increased and at the same time more neutrons react with the lithium, thus decreasing the neutron flux slightly. This decrease is on the order of 20 %.

As for the multiplier performance, it was found that a beryllium layer at the back of the breeder achieves a higher TBR than at the front. Again, this result was unexpected but can be explained by the fact that Be can also act as a reflector. Figure 4.1 shows that a multiplier at the front is only useful at high thicknesses. Note that the breeder thickness is fixed, thus, a larger multiplier thickness means less shielding material. This effect can be explained by a changing neutron energy spectrum. Most neutrons have intermediate energies of around tens of keV, The (n,2n) multiplication is, however, only active for high neutron energies above around 3 MeV. Therefore a majority of the neutrons get elastically scattered giving them a change to interact with the breeder material.

4.2. LiPb-concept (Lithium-lead)

the LiPb-concept was studied using the same approach. Figure 4.2 shows that both the shielding performance and the TBR are worse than for those the Li-concept. Due to the short breeder distance the local TBR values of LiPb reach a maximum of around 0.25 at the benchmark shielding performance, more than a factor of 2 lower than the Li-concept.

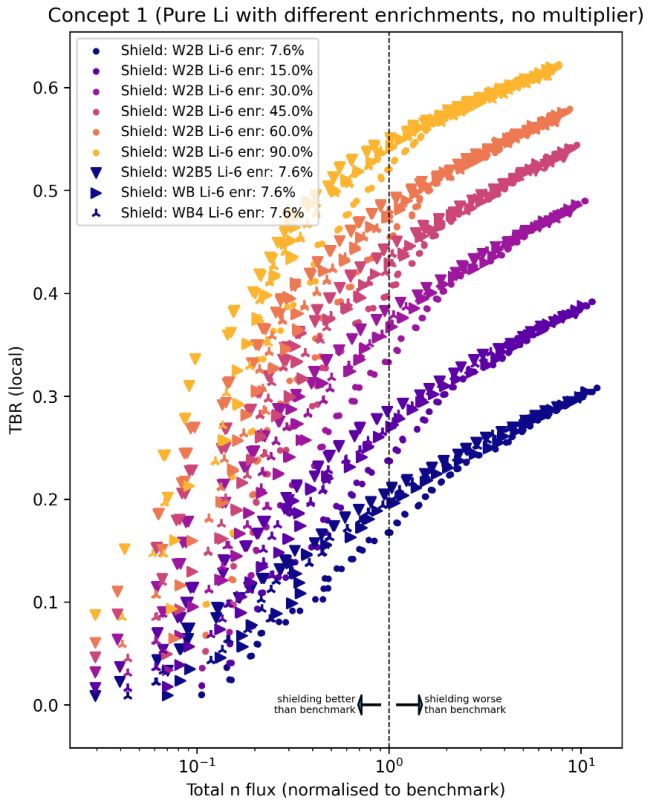

Figure 9: TBR vs total neutron flux after the VV and at the beginning of the HTS magnet for all designs of the Li-concept with no multiplier. Colours represent the enrichment level. The markers show different shielding materials.

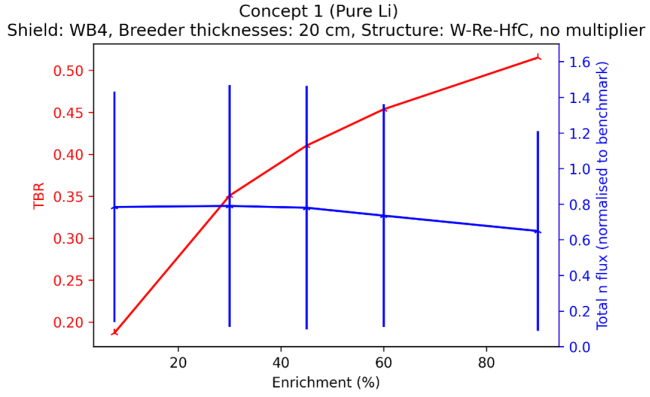

Figure 10: TBR/total neutron flux vs enrichment.

For different enrichment levels (cf. Fig. 4.2) the same trends as for the Li-concept are observed, namely the TBR increases and the neutron flux decreases.

4.3. Comparison of Structural Materials

No significant difference has been found due to the influence of the structural material for the Li-concept. The LiPb-concept has only been tested with one structural material. Figure 4.3 shows the TBR vs shielding for two different structural materials for the Li-concept. The points mostly overlap closely. Given the statistical uncertainty the differences are negligible. Both structural materials are used interchangeably for the neutronics studies.

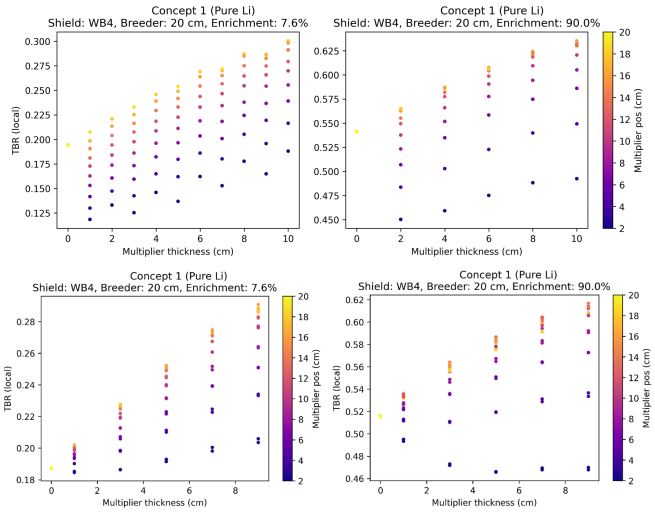

Figure 11: Multiplier performance for natural lithium (left) and lithium with a highly enriched Li-6 content (right).

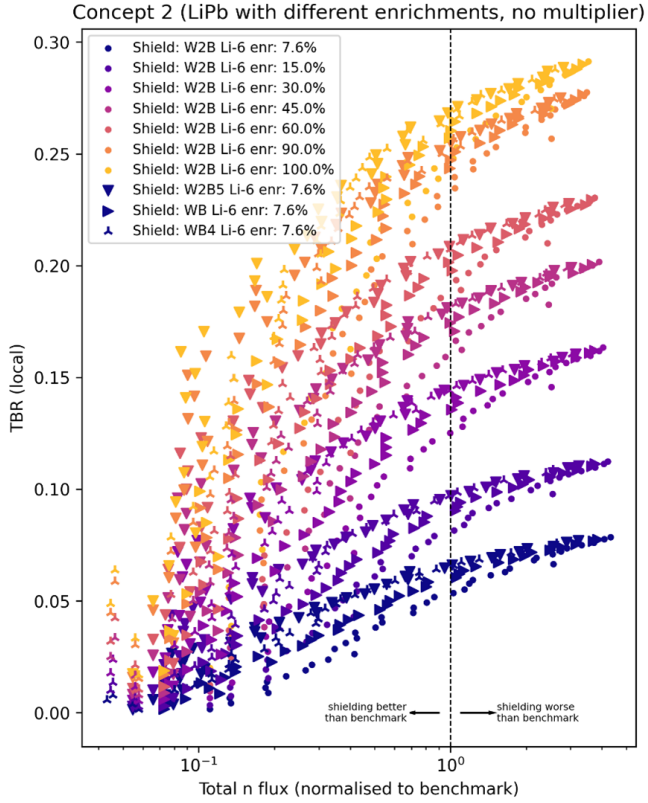

Figure 12: TBR vs total neutron flux after the VV and at the beginning of the HTS magnet for all designs of the LiPb-concept with no multiplier. Colours represent the enrichment level. The markers show different shielding materials.

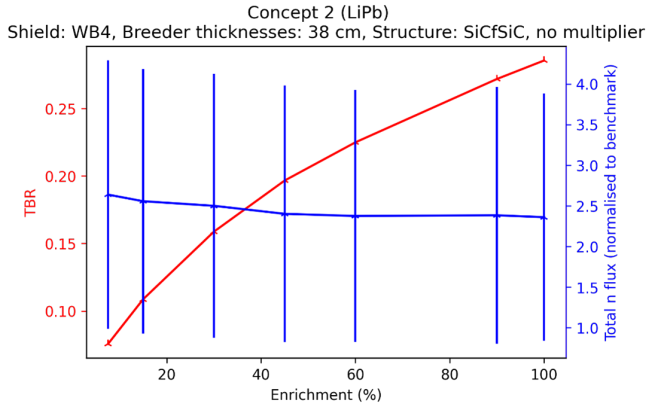

Figure 13: TBR/total neutron flux vs enrichment. Note that the neutron flux has high statistical uncertainty.

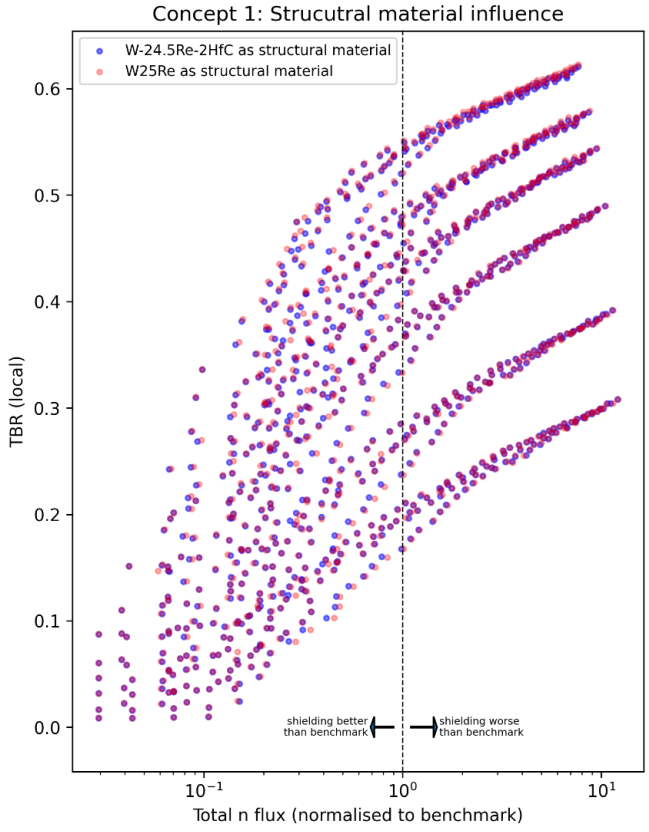

Figure 14: TBR vs total neutron flux after the VV and at the beginning of the HTS magnet for two different structural materials.

4.4. Global TBR

A 3D simulation has been performed to obtain a global TBR for a generic spherical tokamak. The results are shown in Table 1. The correction factor between local and global TBR_{IB} is design-dependent and between 0.23 and 0.41. A maximum of 0.135 additional TBR due to the inboard breeding could be achieved with the Li-concept at 90 % Li-6 enrichment. The results are specific and sensitive to the reactor geometry.

Table 1
TBR results. Local TBR and global TBR_{IB} values are directly available from the designs described study. The global TBR_{IB+OB} was calculated with an exemplary outboard blanket design that delivers an additional TBR of 1.02 to 1.11.

Design	Li-6 Enrichment	Local TBR	Global TBR_{IB}	Global TBR_{IB+OB}
Benchmark	-	-	-	1.072
Best Li-concept with natural enrichment	natural	0.095	0.039	1.093
Best Li-concept design with multiplier and high enrichment	90%	0.426	0.135	1.157
Best LiPb concept with natural enrichment	natural	0.031	0.007	1.113
Best LiPb concept with high enrichment	100%	0.179	0.048	1.135

4.5. Comparison of concepts

The LiPb-concept has a low local TBR with the Pareto curve being lower by a factor of more than 10 compared to the Li-concept. In the confined IB space, the breeding thickness is very short compared to OB; the Li-concept with its higher Li-6 content has an advantage over the LiPb-concept. The (n,elastic) cross-section of LiPb is much higher than of Li (about a factor 6 at 1 MeV) and because the simple geometry allows neutrons to escape out its sides significantly more neutrons are lost due to scattering for LiPb. The global TBR values are not affected by this issue.

Even though the LiPb-concept has many advantages in the other design aspects (see. Section 6) it can only provide a small boost to the global TBR, which stands in comparison to the increase in complexity of adding a liquid breeder into the central column. Below we focus on designs based on the Li-concept.

Using the tungsten boride shielding materials it is possible to outperform the benchmark shielding for the neutron fluxes and still obtain tritium breeding. Four possible design choices have been selected that outperform total and fast neutron fluxes of the benchmark. For each concept, one design without Li-6 enrichment and one design with high Li-6 enrichment have been selected. Both designs maximise TBR while satisfying the flux conditions. The designs are listed in Table 2. The design with enrichment has a more than four times higher local TBR. For the Li-concept, the designs use a Be layer in the middle of the breeder working as a multiplier and reflector.

4.6. Thermal Analysis

The results are summarised in Tables 3 and 4. Additionally, the full heat transfer into the coolant was summed,

Table 2
High and low enrichment lithium designs compared with benchmark (all neutron fluxes are given for the position after the VV and at the beginning of the HTS magnet)

Design	Layer thickness (cm)	Material	Li enrichment	Local TBR	Total neutron flux (n/cm^2)	Fast neutron flux (n/cm^2)	Photon flux (p/cm^2)
Benchmark	0.3 45 15 40	Tungsten Shield Steel vacuum vessel HTS magnet	-	-	1.1e-06	3.0e-07	1.9e-07
Best Li-concept design with multiplier and natural lithium	0.3 0.3 6 1 2 0.3 34.1 1 15 40	Tungsten W-24.5Re-2HfC Li $Be_{12}Ti$ Li W-24.5Re-2HfC W_2B_5 Vacuum gap Steel vacuum vessel HTS magnet	natural	0.095	8.1e-07	2.4e-07	3.4e-07
Best Li-concept design with multiplier and high enrichment	0.3 0.3 4 7 2 0.3 30.1 1 15 40	Tungsten W-24.5Re-2HfC Li $Be_{12}Ti$ Li W-24.5Re-2HfC W_2B_5 Vacuum gap Steel vacuum vessel HTS magnet	90%	0.426	1.0e-06	2.8e-07	4.3e-07
Best LiPb-concept design and natural lithium	0.3 0.2 14 0.2 29.3 1 15 40	Tungsten SiC_f/SiC LiPb SiC_f/SiC W_2B_5 Vacuum gap Steel vacuum vessel HTS magnet	natural	0.031	9.0e-07	1.9e-07	3.2e-07
Best LiPb-concept design and high enrichment	0.3 0.2 14 0.2 29.3 1 15 40	Tungsten SiC_f/SiC LiPb SiC_f/SiC W_2B_5 Vacuum gap Steel vacuum vessel HTS magnet	100%	0.179	9.8e-07	2.2e-07	3.5e-07

including the heat through components R14, R15, R16 and R17, plus the volumetric neutronic heating rate of $4327\,J\,kg^{-1}$ for the Li-concept and $60\,J\,kg^{-1}$ for the LiPb-concept. Assuming an allowable temperature increase in the lithium coolant of 100 K, $450\,kg\,s^{-1}$ flow rate for the Li-concept and a LiPb coolant of 100 K, $8000\,kg\,s^{-1}$ flow rate for the LiPb-concept would be required for the central column. This coolant flow rate is high but not unreasonable, e.g. the ARIES-ST design assumed a flow rate of $47\,450\,kg\,s^{-1}$ [49].

4.7. Structural Analysis

Li-concept For the Li-concept, the simplified geometry assumes a large radius of 1.4 m, bounding the whole central column of a tokamak, with no support or benefit from breaking the design down into modules arrayed circumferentially

Table 3
Volumetric heat generation rates

Concept	Q1 (J/Kg)	Q2 (J/Kg)	Q3 (J/Kg)	Q4 (J/Kg)	Q5 (J/Kg)	Q6 (J/Kg)
Li	0.2	400	275	13	13	0
LiPb	16.4	6	N/A	6.3	27	0

Table 4
Resulting temperatures and critical heat flows

Component	Li-concept	LiPb-concept
First wall	1210 K	1465 K
Front structure	1185 K	1310 K
Coolant	1000 K	1000 K
Multiplier	1135 K	N/A
Rear structure	1000 K	1005 K
Shield Temperature	1035 K	1143 K
Heat flow to HTS magnets	35 kW	35 kW

around the column, meaning that the stresses will easily bound those in a practical design. The pressure P is chosen to be 200 kPa, which corresponds to 100 kPa to account for the fact that the pressure is relative to vacuum, and an additional 100 kPa which accounts for hydrostatic pressure in a liquid lithium coolant over a height of 15 m. Given the thickness of 3 mm, this leads to a stress of 93 MPa.

At the peak temperature of 1185 K as calculated in the thermal analysis, W-25Re has a yield strength of around 650 MPa [2], which is believed to be similar for the other tungsten alloy of W-24.5Re-2HfC. This then leads to a reserve factor of about 7, indicating plenty of structural margin at the specified thickness.

LiPb-concept For the LiPb-concept, the coolant is significantly more dense, leading to much higher hydrostatic pressures, and the thickness is also lower due to the poor thermal conductivity of SiC_f/SiC compared to the tungsten alloys. This means that a radius of 0.2 m is required for the concept, which would be realised by arranging a number of modules around the perimeter of the central column, limiting the radius in each module. This should be considered further for a detailed design. Using this radius and a thickness of 2 mm, a stress of 146 MPa is found. Using a lower bound strength for SiC_f/SiC of 225 MPa [2], a reserve factor or 1.5 is calculated, indicating there is still acceptable margin for this design.

5. Discussion

The thermal assessment shows that the high temperature concepts using a coolant temperature of 1000 K and structural materials (tungsten-rhenium alloy/SiC_f/SiC) with high maximum continuous service temperatures are well suited to breeding in the central column. The limiting temperatures occur at the plasma surface, with the tungsten armour operating at or slightly above the recrystallisation temperature, and well in excess of the ductile-to-brittle transition. Temperatures in the LiPb-concept are generally slightly higher than the Li-concept and this is considered consistent with the reduction in shielding performance in the SiC_f/SiC and breeding in the Lead-Lithium, when compared to the Tungsten-Rhenium and Lithium in the Li-concept.

A full thermal-hydraulic assessment of the design has not been completed, and initial coolant flow rates are high. An assessment of the overall power requirement to provide coolant at the required flow rates should be undertaken to support feasibility assessment of these concepts.

For the design points presented, no allowance has been made for vacuum vessel cooling. This represents a pessimistic assumption, and should the heat flows of 35 kW and 45 kW respectively for Concepts 1 and 2 be considered too high, a cooling system in the vacuum vessel could further reduce the heat reaching the magnets.

Structurally, the thicknesses of materials chosen for the concepts are sufficient, but with considerably more margin in the design for the Li-concept than the LiPb-concept.

As mentioned in Section 2.1.3, the flow of liquid metals can lead to large MHD pressure losses due to interactions with the poloidal and toroidal fields. These losses are most problematic where the flow and field lines are perpendicular and so specific design choices can be used to mediate them. However, coatings may also be used to decouple the liquid metal from the structural material, also reducing losses [14]. These coatings are electrical insulators on the order of micrometres (μm). Oxides such as CaO have been selected for use. Chemical compatibility between the coolant / breeding material and with the structural material is an important design parameter, over expected and off-design temperature ranges. Self-healing of any defects which might occur during operation are considered essential for reliability. Thermal insulations also cause elevated system temperatures that may cause issues in thermal design space [45]. The electrical conductivity for tungsten-rhenium is $26 \times 10^{-6}\,\Omega\,\mathrm{cm}$ compared to that of tungsten, $7.5 \times 10^{-6}\,\Omega\,\mathrm{cm}$ [9, 30]. These values are comparable, and so it is likely that an electrically insulating coating would still be required to account for MHD pressure drops.

As noted in Section 2.1.3, beryllium and lead offer different characteristics for use as neutron multipliers. Whilst lead is reasonably compatible with lithium and can be used as a combined coolant, breeding material and multiplier, in the case of lithium-lead self-cooled designs, its neutron multiplication properties are not as good as those of beryllium. However, the need to isolate elemental beryllium from lithium significantly complicates its use. Ultimately, both materials have limitations that complicate and potentially preclude their use, especially in the confined space inboard of the reactor. [12] notes several important basic characteristics of candidate multiplier materials, particularly their safety (indexed against ease of disposal), their activation characteristics and their availability. Whilst neither lead nor beryllium raise showstoppers for any of these characteristics,

lead is noted to produce polonium-210 in limited quantities, but this is not painted as a significant concern. Whilst lead cannot be disposed of in as large concentrations as beryllium [12], the cost of beryllium is considerable due to its toxicity and the resultant precautions that need to be taken during production [28].

6. Conclusions

In this project, two concepts for arrangements of materials and coolants in the central column were produced, with the aim being to carry out tritium breeding in the central column in addition to the other requirements of shielding and cooling. The two concepts made use of novel arrangements of multi-purpose materials, and both used a self-cooled design wherein the coolant is also the breeder material. These design choices were made in order to make maximum use of the constrained space in the central column. Both concepts were run for a large number of size and material combination permutations, with the aim of extracting both the pareto-optimal trade-off curve between shielding performance and Tritium breeding, and also the details of promising design points. The key results from the project are shown in Section 4.1 and 4.2. These sections show the trade-off between shielding performance and TBR for the two concepts. They indicate that for the pure Lithium the Li-concept design, local TBRs of approximately 0.6 are possible while maintaining the shielding performance of the baseline design. The potential TBR values for the LiPb-concept are smaller however, giving a local TBR of up to around 0.25. A full 3D neutronics simulation of the reactor with and without an inboard breeder blanket has been performed and the increase is 0.135 and 0.048 for the Li- and LiPb-concept, respectively.

For both concepts, the designs producing the highest TBR for a given level of shielding were those that contained the highest Li-6 enriched lithium, with natural lithium giving a factor of at least three reduction in TBR compared with very highly enriched lithium. This conclusion was not unexpected in the limited space environment of the central column, with the most breeding occurring as more lithium-6 is added to the constrained space. Both designs also showed a clear trade-off between shielding performance and TBR, with more room dedicated to lithium leading to higher TBR and poorer shielding. The structural and shielding material variants made little difference to the results, as they offered relatively similar performance to each other. The TBR has been assessed in a full 3D model to find the improvement in global TBR_{IB+OB} vs local TBR. The overall conclusions from this project are that using a pure lithium breeding design in the central column may offer a sufficient improvement in global TBR (0.04 to 0.14), high enough for further consideration. LiPb performed worse (0.01 to 0.05) but if the breeder of the OB blanket is chosen to be LiPb, it is recommended to consider this option for IB breeding. LiPb offers improved material compatibility and handling compared to the Li concept. A next step would be to study the trade-off of gained TBR vs complexity and cost with a system level economic model.

Acknowledgement

We would like to thank Frazer-Nash Consultancy and in particular Greg Nelson and Lewis Farrimond who helped in the conceptualisation and thermal modelling for this project. We would like to thank UKAEA for funding this design study. We would also like to thank Max Karous for a review of the neutronics simulation.

7. Bibliography

References

[1] Akahoshi, E., Matsunaga, M., Kimura, K., Nakamura, K., Balden, M., Hishinuma, Y., Chikada, T., 2020. Corrosion tests of multilayer ceramic coatings in liquid lithium-lead. Fusion Engineering and Design 160, 111874. URL: https://www.sciencedirect.com/science/article/pii/S0920379620304221, doi:https://doi.org/10.1016/j.fusengdes.2020.111874.

[2] Ansys, 2021. Granta selector 2021 r1 version 21.1.1 .

[3] Athanasakis, M., Ivanov, E., del Rio, E., Humphry-Baker, S.A., 2020. A high temperature w2b–w composite for fusion reactor shielding. Journal of Nuclear Materials 532, 152062. URL: https://www.sciencedirect.com/science/article/pii/S0022311519315326, doi:https://doi.org/10.1016/j.jnucmat.2020.152062.

[4] Chadwick, M., Herman, M., Obložinský, P., et al., 2011. ENDF/B-VII.1 nuclear data for science and technology: Cross sections, covariances, fission product yields and decay data. Nuclear Data Sheets 112, 2887 – 2996. URL: https://www.sciencedirect.com/science/article/pii/S009037521100113X, doi:10.1016/j.nds.2011.11.002. special Issue on ENDF/B-VII.1 Library.

[5] Costley, A., Hugill, J., Buxton, P., 2015. On the power and size of tokamak fusion pilot plants and reactors. Nuclear Fusion 55, 033001. URL: https://dx.doi.org/10.1088/0029-5515/55/3/033001, doi:10.1088/0029-5515/55/3/033001.

[6] Crowther, S., Farrimond, L., Slevin, E., 2022. Fnc013725-52893r issue 2 - low power consumption breeder blanket concept study .

[7] Deck, C., Jacobsen, G., Sheeder, J., Gutierrez, O., Zhang, J., Stone, J., Khalifa, H., Back, C., 2015. Characterization of sic–sic composites for accident tolerant fuel cladding. Journal of Nuclear Materials 466, 667–681.

[8] Dong, X., Shin, Y.C., 2018. Predictions of thermal conductivity and degradation of irradiated sic/sic composites by materials-genome-based multiscale modeling. Journal of Nuclear Materials 512, 268–275.

[9] Elert, G., . The physics factbook. URL: https://hypertextbook.com/facts/2004/DeannaStewart.shtm.

[10] Fischer, U., Bachmann, C., Jaboulay, J., Moro, F., Palermo, I., Pereslavtsev, P., Villari, R., 2016. Neutronic performance issues of the breeding blanket options for the european demo fusion power plant. Fusion Engineering and Design 109-111, 1458–1463.

[11] Fukada, S., Terai, T., Konishi, S., Katayama, K., Chikada, T., Edao, Y., Muroga, T., Shimada, M., Merrill, B., Sze, D.K., 2013. Clarification of tritium behavior in pb-li blanket system. MATERIALS TRANSACTIONS 54, 425–429. doi:10.2320/matertrans.MG201203.

[12] Hernández, F., Pereslavtsev, P., 2018. First principles review of options for tritium breeder and neutron multiplier materials for breeding blankets in fusion reactors. Fusion Engineering and Design 137, 243–256.

[13] Howlett, C., Underhill, R., 2021. Fnc 60148/49312r - nuclear heat transfer and passive cooling, volume 5: Liquid metal thermal hydraulics. IMechE .

[14] Ibano, K., Kasada, R., Yamamoto, Y., Konishi, S., 2013. Neutronics and pumping power analyses on the tokamak reactor for the fusion-biomass hybrid concept. Fusion Engineering and Design 88, 2881–2884.

[15] Ihli, T., Basu, T., Giancarli, L., Konishi, S., Malang, S., Najmabadi, F., Nishio, S., Raffray, A., Rao, C., Sagara, A., Wu, Y., 2008. Review of blanket designs for advanced fusion reactors. Fusion Engineering and Design 83, 912–919.

[16] Isobe, K., Yamanishi, T., Konishi, S., 2010. Tritium permeation behavior in sic/sic composites. Fusion Engineering and Design 85, 1012–1015.

[17] Katoh, Y., Nozawa, T., Shih, C., Ozawa, K., Koyanagi, T., Porter, W., Snead, L.L., 2015. High-dose neutron irradiation of hi-nicalon type s silicon carbide composites. part 2: Mechanical and physical properties. Journal of Nuclear Materials 462, 450–457.

[18] Katoh, Y., Snead, L., Henager, C., Nozawa, T., Hinoki, T., Iveković, A., Novak, S., d. Vicente, S.G., 2014. Current status and recent research achievements in sic/sic composites. Journal of Nuclear Materials 455, 387–397.

[19] Khairulin, R., Abdullaev, R., Stankus, S., Agazhanov, A., Savchenko, I., 2016. Volumetric properties of lithium–lead melts. International Journal of Thermophysics 38.

[20] Klopp, W.D., Raffo, P.L., Witzke, W.R., 1971. Strengthening of molybdenum and tungsten alloys with hfc. Journal of Metals 23, 27–38.

[21] Koning, A., Rochman, D., Sublet, J.C., Dzysiuk, N., Fleming, M., van der Marck, S., 2019. Tendl: Complete nuclear data library for innovative nuclear science and technology. Nuclear Data Sheets 155, 1–55. URL: https://www.sciencedirect.com/science/article/pii/S009037521930002X, doi:https://doi.org/10.1016/j.nds.2019.01.002. special Issue on Nuclear Reaction Data.

[22] Konishi, S., Enoeda, M., Nakamichi, M., Hoshino2, T., Ying, A., Sharafat, S., Smolentsev, S., 2017. Functional materials for breeding blankets—status and developments 57.

[23] Koyanagi, T., Katoh, Y., George, J., Deck, C.P., 2018. Issue update to LWR SiC/SiC cladding handbook of properties. Technical Report. Oak Ridge National Lab.(ORNL), Oak Ridge, TN (United States).

[24] Krasko, G.L., 1997. Effect of impurities on the electronic structure of grain boundaries and intergranular cohesion in iron and tungsten. Materials Science and Engineering: A 234-236, 1071–1074. URL: https://www.sciencedirect.com/science/article/pii/S0921509397004176, doi:https://doi.org/10.1016/S0921-5093(97)00417-6.

[25] L, R.P., 1969. Yielding and fracture in tungsten and tungsten-rhenium alloys. Journal of the Less Common Metals , 113–149.

[26] Leonhardt, T., 2009. Properties of tungsten-rhenium and tungsten-rhenium with hafnium carbide. Refractory Metals Research 61, 68–71.

[27] M. R. Gilbert, J.C.S., Turner, A., 2016. Handbook of activation, transmutation, and radiation damage properties of the elements and of iter mateirals simulated using fispact-ii & tendl-2025; iter fw armour focus .

[28] Malang, S., Mattas, R., 1995. Comparison of lithium and the eutectic lead-lithium alloy, two candidate liquid metal breeder materials for self-cooled blankets. Fusion Engineering and Design 27, 399–406.

[29] Mastry, J.A.D., 1967. Corrosion studies of tungsten, molybdenum, and rhenium in lithium. Nuclear Applications 3, 127–134.

[30] MatWeb, . W-25 re tungsten rhenium alloy, annealed. URL: https://www.matweb.com/search/datasheet.aspx?matguid=ec5e2badc6cf467191fd545182b139ef&ckck=1.

[31] "Meng, X., Zuo, G., Sun, Z., Xu, W., Huang, M., Xu, C., Qian, Y., Hu, W., Hu, J., Deng, H., 2018. "compatibility of molybdenum, tungsten, and 304 stainless steel in static liquid lithium under high vacuum". "Plasma Physics Reports" 44, "671–677".

[32] Moir, R.W., d. Lee, J., Fulton, F.J., Huegel, F., s. Neef, W., Sherwood, A.E., Whitley, R.H., Wong, C.P.C., DeVan, J.H., Grimes, W.R., Chose, S.K., 1985. Design of a helium-cooled molten-salt fusion breeder. Fusion technology 8.

[33] Moriyama, H., Tanaka, S., Sze, D., Reimann, J., Terlain, A., 1995. Tritium recovery from liquid metals. Fusion Engineering and Design 28, 226–239.

[34] Muroga, T., Chen, J., Chernov, V., Kurtz, R., Le Flem, M., 2014. Present status of vanadium alloys for fusion applications. Journal of Nuclear Materials 455, 263–268. URL: https://www.sciencedirect.com/science/article/pii/S0022311514003821, doi:https://doi.org/10.1016/j.jnucmat.2014.06.025. proceedings of the 16th International Conference on Fusion Reactor Materials (ICFRM-16).

[35] Nicholas, T., Davis, T., Federici, F., Leland, J., Patel, B., Vincent, C., Ward, S., 2021. Re-examining the role of nuclear fusion in a renewables-based energy mix. Energy Policy 149, 112043. URL: https://www.sciencedirect.com/science/article/pii/S0301421520307540, doi:https://doi.org/10.1016/j.enpol.2020.112043.

[36] Parida, S.K., Nagaraj, S., Venkatesh, M., Sudha, R., Sekhar, K.R., Ramaseshan, R., Ganesan, R., 2019. Studies on chemical compatibility of steels with liquid lithium. Journal of Nuclear Materials 526, 151761. URL: https://www.sciencedirect.com/science/article/pii/S0022311519300376, doi:https://doi.org/10.1016/j.jnucmat.2019.151761.

[37] Park, C., Nozawa, T., Kasada, R., Tosti, S., Konishi, S., Tanigawa, H., 2018. The effect of wall flow velocity on compatibility of high-purity sic materials with liquid pb-li alloy by rotating disc testing for 3000h up to 900°c. Fusion Engineering and Design 136A, 623–627.

[38] Pearson, R., Baus, C., Konishi, S., Mukai, K., D'Angiò, A., Takeda, S., 2022. Overview of kyoto fusioneering's scylla© ("self-cooled yuryo lithium-lead advanced") blanket for commercial fusion reactors. IEEE Transactions on Plasma Science 50, 4406–4412. doi:10.1109/TPS.2022.3211410.

[39] Pint, B.A., Tortorelli, P., Jankowski, A., Hayes, J., Muroga, T., Suzuki, A., Yeliseyeva, O., Chernov, V., 2004. Recent progress in the development of electrically insulating coatings for a liquid lithium blanket. Journal of Nuclear Materials 229-333, 119–124.

[40] Raffo, P.L., 1968. Yielding and fracture in tungsten and tungsten-rhenium alloys .

[41] Ren, C., Fang, Z., Koopman, M., Butler, B., Paramore, J., Middlemas, S., 2018. Methods for improving ductility of tungsten - a review. International Journal of Refractory Metals and Hard Materials 75, 170–183. URL: https://www.sciencedirect.com/science/article/pii/S0263436818300659, doi:https://doi.org/10.1016/j.ijrmhm.2018.04.012.

[42] Romano, P.K., Horelik, N.E., Herman, B.R., Nelson, A.G., Forget, B., Smith, K., 2015. Openmc: A state-of-the-art monte carlo code for research and development. Annals of Nuclear Energy 82, 90–97. URL: https://www.sciencedirect.com/science/article/pii/S030645491400379X, doi:https://doi.org/10.1016/j.anucene.2014.07.048. joint International Conference on Supercomputing in Nuclear Applications and Monte Carlo 2013, SNA + MC 2013. Pluri- and Trans-disciplinarity, Towards New Modeling and Numerical Simulation Paradigms.

[43] Saraswati, P.K., 2021. 7 - geochemical proxies of climate and environment. in Foraminiferal Micropaleontology for Understanding Earth's History , 181–236.

[44] Shimakawa, S., Sagawa, H., Kuroda, T., Suzuki, T., Kawamura, H., Takatsu, H., Saito, M., 1995. Estimation of the tritium production and inventory in beryllium 28, 215–219.

[45] Smith, D., Natesan, K., Park, J.H., Reed, C., Mattas, R., 2000. Development of electrically insulating coatings on vanadium alloys for lithium-cooled blankets. Fusion Engineering and Design 51-52, 185–192.

[46] Soto, C., Martínez-Esnaola, J.M., García-Rosales, C., 2016. Thermo-mechanical analysis of a flow channel insert based on a sic-sandwich material concept. Nuclear Materials and Energy 7, 5–11.

[47] Sykes, A., Costley, A., Windsor, C., Asunta, O., Brittles, G., Buxton, P., Chuyanov, V., Connor, J., Gryaznevich, M., Huang, B., Hugill, J., Kukushkin, A., Kingham, D., Langtry, A., McNamara, S., Morgan, J., Noonan, P., Ross, J., Shevchenko, V., Slade, R., Smith, G., 2017.

Compact fusion energy based on the spherical tokamak. Nuclear Fusion 58, 016039. URL: https://dx.doi.org/10.1088/1741-4326/aa8c8d, doi:10.1088/1741-4326/aa8c8d.

[48] Tillack, M., Bringuier, S., Holmes, I., Holland, L., Santos-Novais, F., Maldonado, G., 2022. Gambl – a dual-cooled fusion blanket using sic-based structures. Fusion Engineering and Design 180, 113155. URL: https://www.sciencedirect.com/science/article/pii/S092037962200151X, doi:https://doi.org/10.1016/j.fusengdes.2022.113155.

[49] Tillack, M., Wang, X., Pulsifer, J., Malang, S., Sze, D., Billone, M., Sviatoslavsky, I., 2003. Fusion power core engineering for the aries-st power plant. Fusion Engineering and Design 65, 215–261. URL: https://www.sciencedirect.com/science/article/pii/S0920379602003058, doi:https://doi.org/10.1016/S0920-3796(02)00305-8.

[50] UKAEA, . Fispact reference input spectra. URL: https://fispact.ukaea.uk/wiki/Reference_input_spectra.

[51] Underhill, R., Olive, A., 2021. Fnc 60148/50158r - nuclear heat transfer and passive cooling - study a: Liquid metal cfd modelling of the tall-3d test facility. IMechE .

[52] Windsor, C., Marshall, J., Morgan, J., Fair, J., Smith, G., Rajczyk-Wryk, A., Tarragó, J., 2018. Design of cemented tungsten carbide and boride-containing shields for a fusion power plant. Nuclear Fusion 58, 076014. URL: https://dx.doi.org/10.1088/1741-4326/aabdb0, doi:10.1088/1741-4326/aabdb0.

[53] Windsor, C.G., Astbury, J.A., Davidson, J.J., McFadzean, C.J., G. Morgan, C.L.W., Humphry-Baker, S.A., 2021. Tungsten boride shields in a spherical tokamak fusion power plant. Nuclear Fusion 61.

[54] Yamamoto, Y., Murakami, Y., Yamaguchi, H., Yamamoto, T., Yonetsu, D., Noborio, K., Konishi, S., 2016. Re-evaluation of sic permeation coefficients at high temperatures. Fusion Engineering and Design 109-111, 1286–1290.

[55] Zhang, D., Meng, X., Zuo, G., Huang, M., Li, L., Xu, W., Li, C., Tang, Z., Yuan, J., Liu, Y., Cao, X., Hu, J., 2021. Study of the corrosion characteristics of 304 and 316l stainless steel in the static liquid lithium. Journal of Nuclear Materials 553, 153032. URL: https://www.sciencedirect.com/science/article/pii/S0022311521002555, doi:https://doi.org/10.1016/j.jnucmat.2021.153032.